Est. 1984

ORIENTAL JOURNAL OF CHEMISTRY
An International Open Access, Peer Reviewed Research Journal

www.orientjchem.org

ISSN: 0970-020 X
CODEN: OJCHEG
2021, Vol. 37, No.(5):
Pg. 1139-1145

Investigation of Minerals Substituted Hydroxyapatite based Nanocomposite Coated Titanium Implant for Bone Tissue Engineering Applications

DHARMAN GOVINDARAJ and MARIAPPAN RAJAN*

Biomaterials in Medicinal Chemistry Lab, Department of Natural Products Chemistry, School of Chemistry, Madurai Kamaraj University, Madurai 625021, India.
*Corresponding author E-mail: rajanm153.chem@mkuniversity.org

http://dx.doi.org/10.13005/ojc/370518

(Received: July 30, 2021; Accepted: October 10, 2021)

ABSTRACT

In this paper, the collagen (Col)@minerals (Sr, Mg, Ce) substituted hydroxyapatite (MHA1)-halloysite nanotubes-single-walled carbon nanotubes (SWCNT) (Col@MHA1-HNT-SWCNT) nanocomposite was coated on the titanium (Ti) implant was investigated using the electrophoretic deposition (EPD) method. The phase and microstructure analysis of the coated samples were characterized using XRD, and SEM-EDAX, respectively. The *Staphylococcus aureus* and *Escherichia coli* strains were tested for antimicrobial activity. The zone of inhibition shows that the Col@MHA1-HNT-SWCNT nanocomposite coating was effective at inhibiting pathogens. The analysis of blood compatibility revealed that the hemolytic ratio was less than 5%, confirming that the nanocomposite were naturally hemocompatible. Furthermore, the cell viability assay using osteoblast-like cells showed excellent cell proliferation and attachments on prepared samples. According to the findings of this research, the Col@MHA1-HNT-SWCNT nanocomposite coating supports bioactivity through fast osteo- compatibility and has greater bacterial resistance, making it necessary for the required biomedical applications.

Keywords: Hydroxyapatite, Osteoblast cell, Hemocompatiblity, Implants.

INTRODUCTION

In recent years, titanium-based implant materials have been subject to many surface treatment methods (acid-etch, anodizing, plasma-spray) and bioactive coatings (wollastonite, magnesium silicates, bioactive glass and hydroxyapatite)[1,2]. Furthermore, the hydroxyapatite (HA) is the most popular material for bone tissue regeneration among bioactive coatings because of its high cytocompatibility, osteo-conductivity and resemblance with the mineral component of the bone. The introduction of mineral ions enhances HA beneficial characteristics.

Due to the biological significance of these elements and the outstanding biocompatibility of native HA bioceramic, mineral substituted

hydroxyapatite (MHA) including various physiological components such as Mg, Ce and Sr may have significant potential in bone tissue regeneration[3,4]. HA and MHA load-bearing applications are still limited due to their poor adhesion strength and weakness. Because of the poor mechanical characteristics of HA, reinforcements such as Ta_2O_5, Ti, ZnO, HNT, CNT, GO and CNF were developed to improve corrosion resistance and mechanical strength. When utilizing HNT the goal is to combine it with a variety of chemicals to create possible scaffolds for tissue and bone development. But the lower resistance to wear and fracture of MHA and HNT-HA leads to crack proliferation that decreases the corrosion resistance[5]. Various HA-based nanocomposites comprised of polymers and carbon-based materials were designed for this purpose. Nowadays, CNT-based materials have been used for many biomedical applications, because of their structure and great mechanical, thermal and electrical characteristics, and high antibacterial and bioactivity. To increase mechanical properties, CNT-based materials, especially SWCNT, have been used as reinforcing agents in nanocomposites. Collagen (Col) is abundant in blood vessels (Type III), ligaments (Type II), and bone (Type I) and it is increasingly employed as a constituent in synthetic bone. It has high biocompatibility to facilitate adhesion and development, as well as biodegradability to be easily absorbed by the body as a natural polymer[6].

Nanocomposite coatings have been developed using a variety of methods including electrodeposition, electrophoretic deposition, sol-gel, and plasma spraying. Among them, the development of several bioceramics, polymer, and nanocomposite coatings was explored for electrophoretic deposition (EPD) because of their cost efficiency, simplicity, and practical design of complicated structures. Also, the ideal material for cartilage rejuvenation must have superior bioactivity, hemocompatibility, ease of processing and sufficient antimicrobial activity. The design and development of a Col@MHA4-HNT-SWCNT nanocomposite was stated in this manuscript. The mixture of Col and SWCNT with MHA1-HNT proved to be a rational technique for the imitation of natural hard tissues since it results in a significant rise in their biocompatibility. As a result, the nanocomposite formed would prospectively be ideal for orthopedic applications.

MATERIALS AND METHODS

Preparation of MHA1 nanoparticles

An ultrasonication assistance wet chemical process was used to produce MHA1 (Sr, Mg, Ce substituted hydroxyapatite) nanoparticles. Calcium nitrate tetrahydrate, strontium nitrate tetrahydrate, magnesium nitrate hexahydrate, cerium nitrate hexahydrate was used as Ca^{2+}, Mg^{2+}, Sr^{2+}, Ce^{3+} (minerals) source, and diammonium hydrogen phosphate was used as PO_4^{3-} source. Dissolving the salts in distilled water produced an equal volume of 1.0 M Ca+ Mg, Sr, Ce and 0.6 M PO_4^{3-} solutions. The pH of the formulations was adjusted to 11.0 with sodium hydroxide solution, and the temperatures of the solutions were raised to 80°C. At a rate of 5.0 mL/min the phosphate solution was slowly introduced to the Ca+ Mg, Sr, Ce solution. During the mixing of the solutions, a precipitated was occurred quickly. After adding sodium hydroxide solution to change the pH of the final solution to 11.0, it was ultrasonically processed for 30 minute. To bind the required number of OH^- ions to the major Ca+M/P molecules, the solutions were aging for one day. After that, the solutions were neutralized with double distilled water before being treated with ethanol. After aging, the solution was filtered through filter paper, cured at 150°C in a drying hot air oven, and crushed in a mortar. Besides, the prepared MHA1 sample was then calcined in a muffle furnace for 4.0 h at 800°C.

Preparation of MHA1-HNT nanoparticles

Firstly, 0.2 g of HNT aqueous solutions was prepared. The HNT solutions were then combined with a 0.6 M fresh $(NH_4)_2HPO_4$ aqueous solution and kept at room temperature with vigorous stirring. A second aqueous solution containing 1.0 M Ca+ Mg, Sr and Ce was also developed and kept continuously stirred at 50°C. Drop by drop, the first mixture HNT+$(NH_4)_2HPO_4$ is added to the Ca+ Mg, Sr, and Ce solution to synthesis. The final mixture was kept at 60°C for one day with constant stirring. After that, the solution was filtered and cleaned with DD water to produce a white powder. Further, the powder samples were dried at 150°C overnight. Following drying and crushing, MHA1-HNT material was obtained. Electrophoretic deposition of MHA1 and MHA1-HNT nanoparticles MHA1 powder was magnetically stirred for 5.0 h in ethanol at a concentration of 0.5 g L^{-1}. Nitric acid

was used to adjust the pH 4.0 of the suspension before EPD. The EPD process was carried out with a steady voltage of 30 V (DC power supply) and a 10 min deposition time. The deposition took place at room temperature, with continuous stirring. Coated samples were sintered at 300°C for two hours with a heating and cooling rate of 3°C/min to improve coating adhesion. The same procedure refers to the coating of MHA1-HNT nanoparticles.

Electrophoretic deposition nanocomposites

Two types of suspensions were prepared to electrophoretically deposit the MHA1-HNT-SWCNT and Col@MHA1-HNT-SWCNT coatings. The bioceramic- SWCNT (MHA1-HNT and SWCNT) of the coatings were in suspension-I, while the polymer-bioceramic compounds (collagen, MHA1-HNT, and SWCNT) were in suspension-II. In a separate beaker, 50 mL of isopropyl alcohol and 1.7 g of MHA1-HNT and 0.5 Wt% SWCNT were mixed to produce suspension-I. In a beaker, 50 mL of isopropyl alcohol, 1.7 g of MHA1-HNT, 0.5 Wt% SWCNT, and 0.05 g of collagen were mixed to produce suspension-II. Suspensions I and II were thoroughly mixed after being agitated ultrasonically for 2.0 hours. To reach a fully stable suspension, the final suspension was agitated ultrasonically for 30 min and magnetically stirred for 6.0 hours. Previous to electrophoretic deposition, each deposition suspension was ultrasonically agitated for 20 minutes. The final operating pH of MHA1-HNT-SWCNT and Col@MHA1-HNT-SWCNT dispersion in isopropyl alcohol medium was 4.0. The electrophoretic deposition was performed using a DC power source at a steady voltage mode of 30 V for 10 min with platinum as the reference electrode (anode) and titanium substrate as the cathode. The inter-electrode distance was kept constant at 1 cm in all electrophoretic deposition experimental. The coated samples were properly removed from out from the EPD cell and cured sideway in the air for 24 h at room temperature.

Physicochemical characterizations

X-ray diffraction (XRD: D8 advanced ECO XRD SSD160) are used to analyze the phase structure of the coating respectively. Scanning electron microscope (SEM ZEISS EVO 18) fitted with an energy dispersive X-ray spectrometer ((EDAX) BRUKER X-Flash 6130) are used to observe the surface morphology and elemental composition of coating samples.

Antibacterial studies

The antibacterial function of prepared samples was examined by the disc diffusion test against *Gram-positive* bacteria (*Staphylococcus aureus* and *Gram-positive* bacteria (*Escherichia coli*. The control was made of Amoxicillin clavanulate. In a petri plate, the nutrient broth mixture was filtered and left to cool for thirty min. The microbial solutions were evenly scrubbed on the agar medium following cooling. The MHA1, MHA1-HNT, MHA1-HNT-SWCNT and Col@MHA1-HNT-SWCNT (25 µg/mL) solutions were placed onto the disc and distributed over the agar media. Later, at 37°C, the samples were inoculated to incubate for one day. The development of the zone over each disc was determined after incubation by using a bacterial zone index.

Hemocompatibility studies

Shortly, the plasma anti-coagulant mixture (1:10) was supplemented with phosphate buffer solution (pH = 7.4). The samples were then soaked in a microfuge tube containing one ml of anti-coagulant plasma solution was placed at RT for two hours. As positive and negative controls, Tyrode (Sigma-Aldrich) and Triton X 100 (Sigma-Aldrich) were used with EDTA as an anticoagulant agent. The incubator solution was centrifugated for 15 min at 3000 rpm, and the optical density of the supernatant solution acquired in the UV spectrometer was recording at 540nm[7].

***In vitro* cell viability**

The cell viability of titanium coatings of MHA1, MHA1-HNT, MHA1-HNT-SWCNT, and Col@MHA1-HNT-SWCNT at different incubation concentrations (25 µg to100 µg) was assessed by MTT assay. The osteoblast-like cells (MG63) were acquired from NCCS, Pune, and were grown DMEM with 10 percentage FBS and 1 percent GIBCO improvement and opioids (100 U/mL streptomycins, 100 mg/mL penicillin) at 37°C in a 5 percentage carbon dioxide atmosphere. The cultured media was altered every day to ensure strong confluency. Developed osteoblast-like cells were rinsed with phosphate buffer solution and removed from their culture plate, and the $1x10^5$ cell/mL cells were grown in 24-well dishes over the specimens to assess cell proliferation at different doses, such as 25 to 100 µg. The control specimen is the same number of osteoblast-like cells plated in each wells plate without the testing specimen. Dimethyl

sulfoxide was applied to the well-dishes after such an implanted time of 24 h and analyzed at 570nm using a UV-spectrophotometer. The percentage of cell viability of the prepared samples was determined using the formula following. Percentage of cell viability = Treated/Control X 100. For microscopic examination, the solution was fully extracted and supernatants after incubation. Statistical analysis All the analysis described in this research was conducted in triplicate and the statistical results were given as an average ± standard deviation by using origin 8.5.

RESULTS AND DISCUSSION

Crystallographic structure of the coatings

The XRD patterns of pure HNT, SWCNT, MHA1, MHA1-HNT, MHA1-HNT-SWCNT, and Col@ MHA1-HNT-SWCNT nanocomposites were shown in Fig.1. The findings revealed that HNT displays diffraction peaks of 24°, 19°, and 11° at two theta values corresponding to the crystal structure (002), (020/110), and (001) existing in its crystalline form (Fig.1a). SWCNT displays high characteristic peaks at angle two theta, 26° referring to the C (002) reflects of the hexagonal graphite form. A further crystal structure at 42° correlated with C (100) graphite diffractions is also identified for SWCNT (Fig.1b). Collagen had a broad peak at 2θ = 10° to 40° but no significant diffraction angle (Fig.1c). The entire collagen has an amorphous phase.

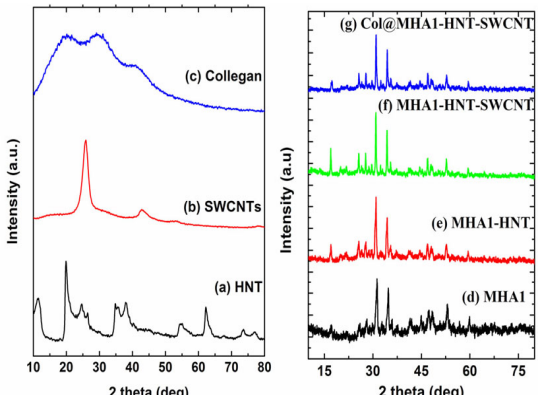

Fig. 1. XRD spectrum of pure (a) HNT, (b) SWCNT, (c) collagen; (d) MHA1, (e) MHA1-HNT, (f) MHA1-HNT-SWCNT, and (g) Col@MHA1-HNT-SWCNT coatings

XRD patterns of MHA1 are seen in Fig.1d. The peak locations of MHA1 have just a minor variation; the peaks of MHA1 have been found at 2θ = 25° (002), 28° (102), 29° (210), 31° (211), 32° (112), 33° (300), 34° (202), 37° (300), 45° (310), 49° (222), 53° (004), and 60° (304). Thus, the XRD patterns acquired are primarily in agreement with JCPDS card no. 09-0432. The diffraction of MHA1 is wider than the standard HA. The findings were already shown in hydroxyapatite co-substituted with minerals[8].

The XRD pattern of the MHA1-HNT is shown in Fig. 3e. The peaks at 2θ= 34°, 2θ= 31°, and 2θ= 25° are attributed to the (202), (002) and (211) reflections of MHA1. The peaks at 2θ= 24° and 2θ= 20° are attributed to the (002) and (100) reflection of HNT. The presence of these peaks further shows the nature of MHA1 and HNT in the MHA1-HNT. MHA1-HNT current XRD pattern resembles the reference's XRD pattern. There were no other impurity peaks found, suggesting that the MHA1-HNT is relatively pure. Fig. 3f shows the XRD patterns of the MHA1-HNT-SWCNT nanocomposite. The characteristic peaks of MHA1-HNT were found at 2θ = 20°, 24°, 25°, 26°, 31°, and 34°, according to JCPDS card no: 024-0033 and JCPDS card no 9-1487, for MHA1-HNT-SWCNT nanocomposite. As a result, SWCNT loading did not affect MHA1-HNT nucleation or formation. Compared to the diffraction patterns of MHA1-HNT, those of MHA1-HNT-SWCNT are very identical, suggesting the effective integration of MHA1- HNT into the SWCNT matrix. Nevertheless, it should be noted that the diffraction peaks of SWCNT could hardly be detected in those of MHA1-HNT-SWCNT nanocomposite, which could be due to the convergence of the main diffraction patterns of SWCNT and MHA1 at 2θ = 26°. The prompt and symmetrical diffraction peaks also reflect the successful crystalline of the MHA1-HNT-SWCNT nanocomposite. In the case of Col@MHA1-HNT-SWCNT nanocomposite, high absorption peaks at 25°, 26°, 31°, and 34° revealed low crystallinity of the MHA1 particle in Col@MHA1-HNT-SWCNT nanocomposite (Fig. 3g)[9]. The XRD pattern shows that the Col@MHA1-HNT-SWCNT nanocomposite coating on titanium was successfully fabricated.

Surface morphology and elemental composition of the coatings

The MHA1-coating surface morphology on the titanium (Fig. 2a) revealed the development of a spherical-like structure with few noticeable cracks. Fig. 2b displays the uniform mixture of rods with spherical-like microstructures identified for MHA1-HNT-coating. MHA1-HNT particles' compact and distinctive shapes are ideal for electrophoretic

deposition and biomedical applications. The MHA1-HNT-SWCNT nanocomposite coating (Fig. 2c) was shown to have a rods MHA1-HNT agglomerate of numerous small rod particles with a diameter up to several tens of nanometers in the SWCNT matrix. Fig. 2d shows that the nanocomposite surface of Col@MHA1-HNT-SWCNT is foam and indicates that the introduction of Col into MHA1-HNT-SWCNT led to the increased coarseness of the hybrid substance accumulated on the substrate of titanium. Compared to the MHA1 coating, the Col@MHA1-HNT-SWCNT nanocomposite coating can help protect the surface; due to its dense and consistent form coating, it has more interaction with the surrounding fluid during implantation and is thus more preferred for apatite accumulation[10].

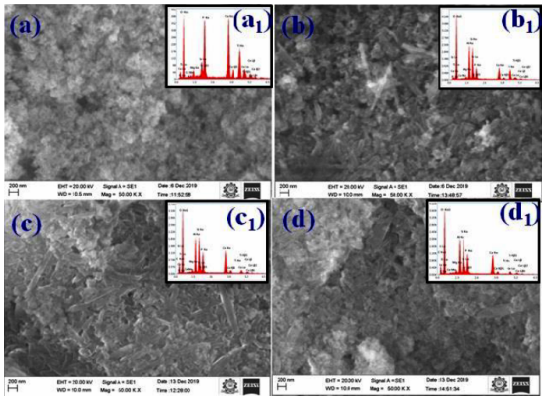

Fig. 2. SEM-EDAX images of the (a-b) MHA1, (c-d) MHA1-HNT, (e-f) MHA1-HNT-SWCNT, and (g-h) Col@MHA4-HNT-SWCNT coatings on titanium

The EDAX spectrum in Fig. 2a1 reveals that the dominant elements on the MHA1 coated surfaces are Ca, Sr, Ce, Mg, O, and P; thus, the spectrum confirms the presence of minerals ions in the coating. Compared to the MHA1 control group, certain additional Al and Si peaks were observed, indicating that HNT had been properly inserted into the MHA1-HNT coating (Fig. 2b1). The EDAX spectrum (Fig. 2c1&d1) of the nanocomposites (MHA1-HNT-SWCNT, and Col@MHA1-HNT-SWCNT) confirm the presence of Ca, Sr, Ce, Mg, Al, Si, O, P, and C elements, which are resulting from the presence of MHA1-HNT and Col-SWCNT composite. As with all the coatings, the titanium peaks contributed to the titanium substrate. The Ca/P ratios of MHA1, MHA1-HNT, MHA1-HNT-SWCNT, and Col@MHA1-HNT-SWCNT, as calculated by the EDAX study, were roughly 1.22, 1.21, 1.27 and 1.26, respectively, significantly lower than the stoichiometric Ca/P ratio of natural apatite (1.67)[11], but similar to that of natural bone, which was assumed to provide biocomposites with greater bioactivity. Furthermore, it was verified that there were no impurities found in the coatings.

In vitro antibacterial activity of the coatings.

Antibacterial efficacy of 32 mm, 33 mm, and 20 mm, 21 mm against *E. coli* and *S. aureus* was demonstrated by MHA1 and MHA1-HNT, respectively (Fig. 3). The antibacterial activity of MHA1-HNT-SWCNT against *E. coli* and *S. aureus* could receive values of 34 mm and 23 mm, respectively, showing that the addition of SWCNT could achieve more effective antibacterial activity than either MHA1 or MHA1-HNT due to the synergistic action of minerals ions and SWCNT in the nanocomposite coating. On the other hand, collagen could considerably increase the antibacterial efficacy of the coating, with the antibacterial activity of Col@MHA1- HNT-SWCNT reaching up to 35 mm and 25 mm against *E. coli* and *S. aureus*, respectively. These findings indicated that the improved antibacterial activity was due to the synergistic bacteria-killing of SWCNT, collagen, and MHA1-HNT in the nanocomposite coating.

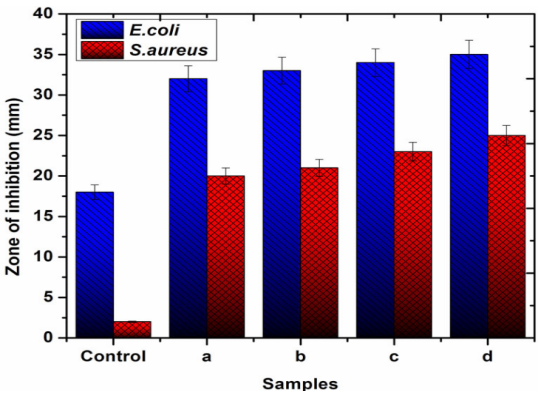

Fig. 3. Antibacterial activity of the (a) MHA1, (b) MHA1-HNT, (c) MHA1-HNT-SWCNT and (d) Col@MHA4-HNT-SWCNT coatings

In vitro hemocompatibility of coatings

Figure 4 is a bar graph that displays the percentage hemolysis values. The values of % hemolysis of MHA1, MHA1-HNT, MHA1-HNT-SWCNT, and Col@MHA1-HNT-SWCNT coatings were 1.9 ± 0.15, 2.5 ± 0.10, 3.3 ± 0.13, and 2.7 ± 0.12, suggesting strong blood- compatibility. Due to SWCNT penetration through the erythrocytes of the plasma membrane, the MHA1-HNT-SWCNT coating demonstrated minimal hemolysis as compared to the MHA1 coating. Nanocomposite has less than 5 percent hemolysis, so it can be observed that the in vivo use of Col@MHA1-HNT-SWCNT coating is comfortable without triggering acute hemolysis[12].

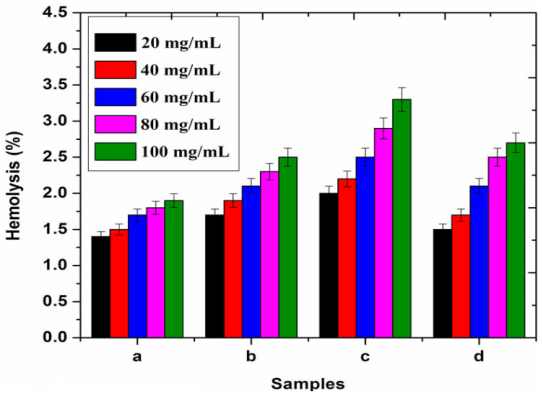

Fig. 4. Hemocompatibility of the (a) MHA1, (b) MHA1-HNT, (c) MHA1-HNT-SWCNT, and (d) Col@MHA4-HNT-SWCNT coatings

In vitro biocompatibility of coatings

The cell viability of the samples was determined using the MTT assay (Fig. 5). It was clear that as sample concentration increased, the number of cells attached to each sample decrease. However, compared to the MHA1-HNT-SWCNT, the cell viability on the Col@MHA1-HNT-SWCNT nanocomposite was noticeably better at 75 to 100 μg, implying that the introduction of collagen into the MHA1-HNT-SWCNT could stimulate MG-63 cell proliferation. So the investigated Col@MHA1-HNT-SWCNT nanocomposite had a cell viability of greater than 70%, it could be declared biocompatible with osteoblast-like cells. The finding of the Col@MHA1-HNT-SWCNT nanocomposite is consistent with previous research showing that mineral phases in combination with natural polymers have a major impact on osteoblast proliferation[13].

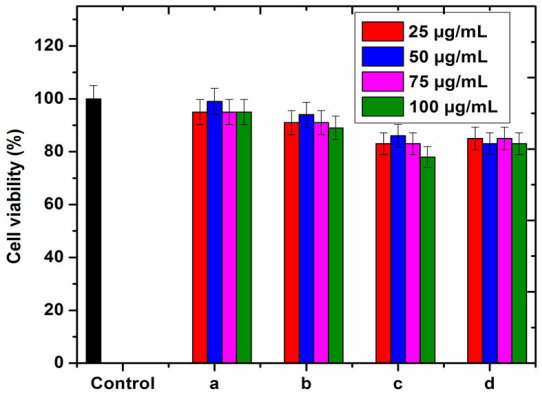

Fig. 5. Cell viability of osteoblast-like cells on 25-100 μg/mL concentrations of (a) MHA1, (b) MHA1-HNT, (c) MHA1-HNT-SWCNT, and (d) Col@MHA4-HNT-SWCNT coatings for 24 hours

Images from phase-contrast microscopy corroborated the MTT report. Fig. 6 shows a concentrated colony of live cells in MHA1 and MHA1-HNT at concentrations ranging from 25-100 μg/mL. These microscopy images show osteoblast-like cells interacting with MHA1-HNT- SWCNT and Col@MHA1-HNT-SWCNT, which displays regular cell adhesion, multiplying, and spreading capability up to concentrations of 25-50 μg/mL for 24 h and the morphology of the cell as a spindle to polygonal with an excellent attachment of cells on the surface of MHA1-HNT-SWCNT and Col@MHA1-HNT-SWCNT nanocomposites. Because of the toxic behavior, 75-100 μg/mL shows less dense cells with a non-adherent nature when compared to lower concentrations. MHA1-HNT-SWCNT and Col@MHA1-HNT-SWCNT at 75-100 μg/mL exhibited up to 18-22 percent toxicity due to leaching of SWCNT, which interfaces with the osteoblast-like cell wall. As previously stated, at concentrations of 75-100 μg/mL, it shows an increased proportion of apoptosis due to SWCNT releasing from the MHA1-HNT matrix, which was validated microscopically. The dead cells have a circular morphology, which is clearly in microscopy photographs. As a result of these in vitro cytocompatibility findings, the Col@MHA1-HNT-SWCNT nanocomposite has good biocompatibility and cell viability at low concentrations and can be used for orthopedic implants.

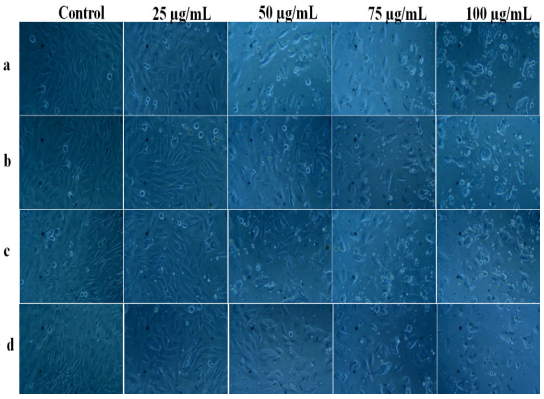

Fig. 6. Optical images of osteoblast-like cells on 25-100 μg/mL concentrations of (a) MHA1, (b) MHA1-HNT, (c) MHA1-HNT-SWCNT, and (d) Col@MHA4-HNT-SWCNT coatings for 24 hours

CONCLUSION

In this study, we used electrophoretic deposition to develop a Col@MHA1-HNT-SWCNT nanocomposite coating on titanium. The XRD and SEM results confirm the formation of

nanocomposite coating on titanium without any impurities. The decrease in bacterial cell growth of Col@MHA1-HNT-SWCNT nanocomposite coating was quantified using the zone of inhibition method. Additionally, hemocompatibility evaluation revealed less than 5% hemolysis, indicating that the coatings have superior blood compatibility. Cell viability assay demonstrated great cell adhesion and proliferations from spindle to polygonal characteristics with lamellipodia and filopodia augmentation for guiding cells on coated metal substrates. As a result, this nanocomposite coating with favorable blood compatibility and better in vitro biocompatibility and antibacterial activity can be effectively used for biomedical purposes.

ACKNOWLEDGEMENT

We are greatly thankful to the following organizations to carry out the analysis work. The South India Textile Research Association for biocompatibility test and XRD, SEM-EDAX kalasalingam academy of research and education.

Conflicts of Interest

The authors declare no conflict of interest.

REFERENCES

1. Mathai, S. An Efficient Electrochemical Approach for Characterization of the Interface Strength of Nano Titania-Silica (TS) Composite Coating on Titanium Implants. *Orient. J. Chem.,* **2018**, *34*, 2180.
2. Aslani, M.; Meskinfam, M.; Aghabozorg, H. In Situ Biomimetic Synthesis of Gelatin-Carbon Nanotube-Hydroxyapatite Biocomposites as Bone Filler. *Orient. J. Chem.*, **2017**, *33*, 235-241.
3. Khadar, Y.S.; Balamurugan, A.; Devarajan, V.P.; Subramanian, R. Hydrothermal synthesis of gadolinium (Gd) doped cerium oxide (CeO_2) nanoparticles: characterization and antibacterial activity. *Orient. J. Chem.,* **2017**, *33*, 2405.
4. Gopi, D.; Murugan, N.; Ramya, S.; Shinyjoy, E.; Kavitha, L.J.R.A., Ball flower like manganese, strontium substituted hydroxyapatite/cerium oxide dual coatings on the AZ91 Mg alloy with improved bioactive and corrosion resistance properties for implant applications. *RSC Advances.*, **2015**, *5*, 27402-27411.
5. Fan, L.; Zhang, J.; Wang, A. In situ generation of sodium alginate/hydroxyapatite/halloysite nanotubes nanocomposite hydrogel beads as drug- controlled release matrices. *Journal of Materials Chemistry B.*, **2013**, *1*, 6261-6270.
6. Yu, L.; Rowe, D.W.; Perera, I.P.; Zhang, J.; Suib, S.L.; Xin, X.; Wei, M.; Intrafibrillar mineralized collagen–hydroxyapatite-based scaffolds for bone regeneration. *ACS applied materials & interfaces.*, **2020**, *12*, 18235-18249.
7. Sakthiguru N.; Manimohan M.; Jaganathan G.; Manivannan K.; Sithique MA., Biologically active Chitosan/ZnO/Acalypha indica leaf extract biocomposite: An investigation of antibacterial, cell proliferation and cell migration aptitude for wound healing application. *Sustain Chem Pharm.*, **2021**, *119*, 100357.
8. Govindaraj, D.; Rajan, M.; Munusamy, M.A.; Alarfaj, A.A.; Sadasivuni, K.K; Kumar, S.S. The synthesis, characterization and in vivo study of mineral substituted hydroxyapatite for prospective bone tissue rejuvenation applications. *Nanomedicine: Nanotechnology, Biology and Medicine.*, **2017**, *13*, 2661-2669.
9. Chen, L.; Hu, J.; Shen, X.; Tong, H. Synthesis and characterization of chitosan–multiwalled carbon nanotubes/hydroxyapatite nanocomposites for bone tissue engineering. *Journal of Materials Science: Materials in Medicine.*, **2013**, *24*, 1843-1851.
10. Deen, I.; Pang, X.; Zhitomirsky, I. Electrophoretic deposition of composite chitosan-halloysite nanotube–hydroxyapatite films. Colloids and Surfaces A: *Physicochemical and Engineering Aspects.*, **2012**, *410*, 38-44.
11. Cacciotti, I. Multisubstituted hydroxyapatite powders and coatings: The influence of the codoping on the hydroxyapatite performances. *International Journal of Applied Ceramic Technology.*, **2019**, *16*, 1864-84.
12. Ferraris, S.; Yamaguchi, S.; Barbani, N.; Cazzola, M.; Cristallini, C.; Miola, M.; Vernè, E. Spriano, S. Bioactive materials: In vitro investigation of different mechanisms of hydroxyapatite precipitation. *Acta biomaterialia.*, **2020**, *102*, 468-480.
13. Armentano, I.; Dottori, M.; Fortunati, E.; Mattioli, S.; Kenny, J.M., Biodegradable polymer matrix nanocomposites for tissue engineering: a review. *Polymer degradation and stability.*, **2010**, *95*, 2126-2146.